Journal of Supramolecular Structure 2:17–31 (1974)

THE QUATERNARY STRUCTURE OF ALFALFA MOSAIC VIRUS

Jan E. Mellema and Hans J. N. van den Berg

Biochemisch Laboratorium, Rijksuniversiteit Leiden, Wassenaarseweg 64, Leiden, The Netherlands

(Received Dec. 5, 1973; accepted Feb. 24, 1974)

From an analysis of electron micrographs of Alfalfa Mosaic Virus (AMV), evidence has been obtained which favors a cylindrical P_6 lattice for the protein coat of the virus. For the analysis use was made of optical diffraction and computer processing of electron images of negatively stained virus particles.

The virus coat exhibits polymorphism. Two kinds of structure were found: a stacked and a helical type. In the stacked type of lattice the unit cells are arranged in staggered rings in such a way that two rings comprise a repeat distance of the structure. The selection rule for the optical diffraction patterns of the stacked form is $l = n + 2m$, in which n is an integer multiple of 3. The layerlines are equally spaced at a distance of approximately $1/80$ Å^{-1}.

In the helical type of lattice these rings of unit cells are transformed into turns of a double helix. The selection rule derived in this case is $l = 6n - 17m$, in which n is an integer multiple of 2. The repeat of the structure is approximately 440 Å.

INTRODUCTION

Preparations of Alfalfa Mosaic Virus (AMV), a RNA containing plant virus, shows a heterogeneity when subjected to sedimentation analysis (1). Electron micrographs of these preparations have revealed a variety of particle shapes ranging from isometric to long tubular structures (2, 3). Both ends of the tubular forms appear to have rounded caps. It has been shown that the average diameter of all tubular forms are the same, suggesting that they have a similar quaternary structure (2, 3). The question then arises how are the protein subunits arranged in the virion and in what way are the different structures topologically related. It is tempting to speculate that the surface lattice is derived from a P_6 lattice rolled up into a cylindrical surface. This would be expected on the theory put forward by Caspar and Klug (4). In this way the capping of the particles as well as the different length classes can easily be explained.

In order to use the technique of optical diffraction for the analysis of the electron images of AMV, the experiments concentrated on a strain, which forms relatively long particles after infection (5). The results obtained favor the existence of a P_6 lattice for the protein coat of the virus. During this study two classes of virus particles were found that differ in their surface lattice. In the so-called stacked type of lattice the morphological units are arranged in staggered rings with two rings in one repeat distance. In the helical type of lattice these annuli are transformed into turns of continuous helices.

Surprisingly the results of these studies point to a rational number for the cylindrical symmetry of the helical structure. The symmetry derived is 2-fold, compared with 3-fold for the stacked type of structure. However, this result is in accordance with the geometrical theory cited by Caspar and Klug (4) as elongation of icosahedral caps by cylindrical structures may proceed according to a 2-, 3-, and 5-fold symmetrical arrangement.

Hull et al. (3) also used optical diffraction for the analysis of their images of AMV. However, although the model they derived was also based on a P_6 lattice, their interpretation of the transforms and their model differ with the results communicated here.

AMV is a simple virus in terms of protein composition, as only one kind of protein is engaged in the architecture of the coat (6). The virus particle is an interesting object for structural studies as it has properties unlike most other viruses. The protein coat does not offer much protection for its RNA, for at neutral pH the RNA is hydrolyzed by the action of RNase (7). Low angle X-ray data suggest an "open" structure for the coat (8). The quaternary structure of the protein coat is able to dissociate by incubation of the virion with its RNA (9).

METHODS

Virus Suspensions

The virus suspensions were kindly supplied by Dr. E. M. J. Jaspars. The isolation was carried out as described by van Vloten-Doting et al. (10). Two AMV strains were used, the Hagedorn and Hanson 425-strain and the VRU strain. The last strain was kindly provided by Dr. Hull (5). In the case of VRU particles a gradient centrifugation was carried out to obtain fractions of relatively long particles. Mg^{2+} aggregates were prepared according to Hull et al. (11).

Electron Microscopy

Micrographs were taken on glass plates (Ilford Special Lantern Contrasty) with a Philips EM 300, operating at 80 KV. The double condensor lens system was used with a spot size of about 10 μ and use was made of the anticontamination device cooled with liquid N_2. The magnification of the microscope was calibrated with a carbon grating replica (Ladd, 21600 lines/cm). For compensating astigmatism and focusing, different areas of the specimen were used as those which were photographed. The specimens were prepared with solutions of 1% uranylacetate (pH 4.2) and 1% sodiumphosphotungstate (pH 7.0) as negative stains. In some experiments the virus was fixed with 1% glutaraldehyde or formaldehyde solutions in 0.1 M phosphate buffer (pH 7.0) for periods of about 15-30

minutes at room temperature. Carbon coated grids were used as specimen support (estimated thickness 100-200 Å). Holey films were prepared according to standard procedures (12). It was found that the morphology of the virus in the electron images was not affected by the grid loading procedures. For example, the same results (see General Observations) were obtained when the virus was present in the staining solution and applied to the grid or when this occurred in two steps, by first allowing the virus to adsorb on the grid followed by the staining.

Image Analysis

The micrographs were analyzed in two ways: by optical diffraction in a coherent system and by computing the numerical Fourier transform after digitizing the image. In the last case one has the possibility of transforming a number of variables derived from the measured intensity values, whereas in the optical diffractometer it is the amplitude transmission function of the micrograph which is transformed (22).

Optical Diffraction. Electron micrographs were analyzed with an optical bench made from commercially available parts (Spindler and Hoyer, Germany). As a light source, a Spectra Physics laser (type 134) was used. The laser beam was expanded with a f = 10 mm microscope objective lens, a pinhole of 50 μ placed in the back-focal plane of the former lens and a f = 400 mm lens with a diameter of about 6 cm. By means of a variable circular aperture the subject could be illuminated with a bundle of parallel light of equal intensity to a maximum diameter of about 1.2 cm. The diffracted arrays were focused with a high quality Fraunhofer lens (f = 1183 mm) on a film (Kodak, Recordak AHU 5460) or could be surveyed on a small screen mounted in the photographic camera (Exakta, Dresden, Germany).

The particles analyzed in the diffractometer were masked off with black adhesive tape on the glass side of the original electron micrograph, which had a magnification of 44,000. No liquid gate was used in the experiments.

The diffractometer constant was determined experimentally and found to correlate well with the theoretical value.

Computer Analysis. The original micrographs were scanned by a Zeiss scanning microscope coupled to a PDP–12 system. The intensity measurements were stored on a disc memory and were made IBM compatible on magnetic tape. Processing of these data took place on the University IBM 370-65 system. As a rule the micrographs were digitized on a square raster with a size of about 8 Å. The projected light beam of the densitometer on the micrograph was circular with a diameter equal to the step size. The Fourier transform algorithm used in the computations has been described by DeRosier and Moore (13). When interpolation in Fourier space was necessary, a bilinear interpolation in both the real and imaginary parts of the Fourier components was carried out.

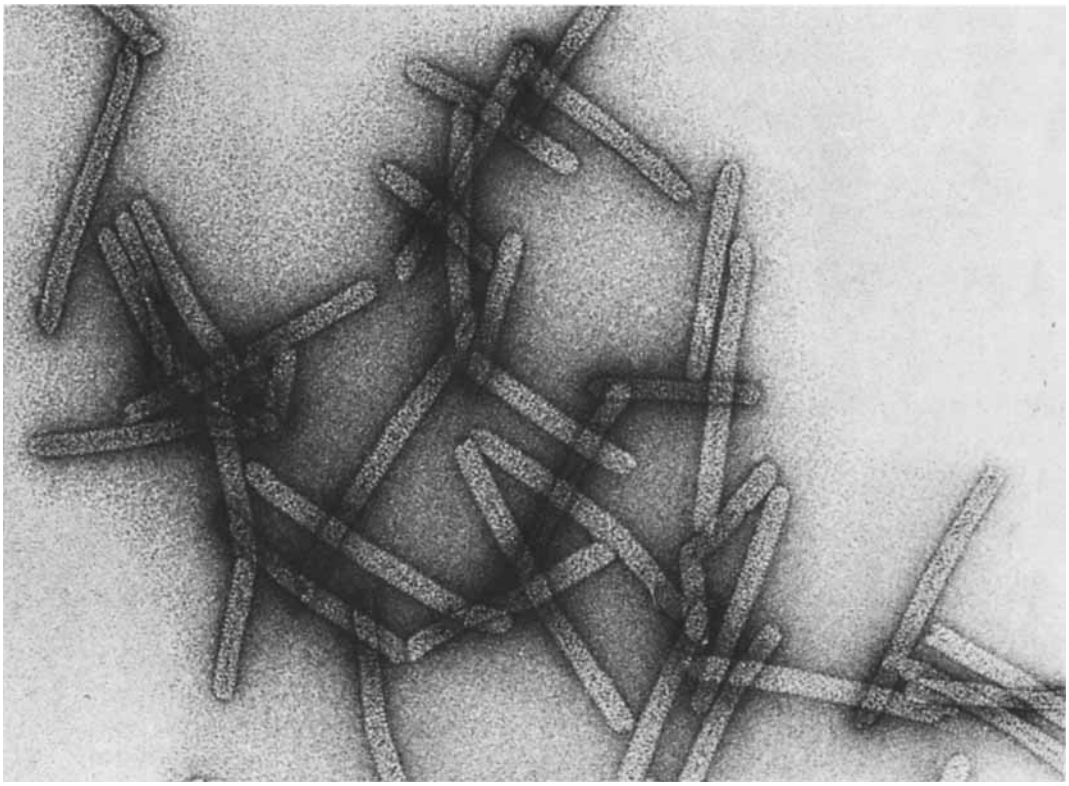

Fig. 1 A micrograph of negatively stained (1% uranylacetate– AMV particles (Strain VRU) on a carbon foil. Magnification: 2.2×10^5.

RESULTS

General Observations

A typical field of negatively stained AMV particles of strain VRU is shown in Fig. 1. As can be observed not all the particles possess the same length. In many cases the particles have a rounded cap at their ends. The longest particles measure about 4000 Å; no dominant length class has been found (5).

The virus particles are not always deposited on the grid as straight rods, but sometimes exhibit bends of nicks. Measurements of the width of the virus particles in a field where both particles suspended in stain over holes and particles lying on carbon were present, yielded average diameters of 150 Å (30 particles analyzed, standard deviation of the mean 10 Å) and 180 Å (30 particles analyzed, standard deviation, 15 Å), respectively. Over holes suspended in stain the diameter of negatively stained particles is smaller than those on carbon, a feature which is common to most images of biological macromolecules. The reason for this difference is probably related to different degrees of flattening. Generally it is assumed that particles on carbon are more flattened than those suspended over holes (15). Preparations of other strains which have been investigated, for example AMV-425, have the same morphology as the ones presented in Fig. 1, but the particles

exhibit a relatively shorter length.

No clear effects of formaldehyde fixation of the virus on this kind of appearance have been found. This conclusion also holds for the optical diffraction patterns of the images of the particles. Images of uranylacetate stained virus particles are of better quality than the phosphotungstate preparations in terms of the observed resolution of the diffraction maxima.

In some cases end-on views of the particles can be obtained by treating the virus suspension with $MgCl_2$ (11). In this way the particles associate side by side and when favorably oriented on the grid, provide a view down the cylindrical axis. An example of such an aggregate is presented in Fig. 2a. For these experiments purified fractions of the bottom component of AMV-425 were used, as it was impossible to find suitable views of the longer VRU aggregates.

It can be observed that the protein coat exhibits a rough hexagonal shape and a projected width of about 40 Å. A number of well preserved end-on views, especially those situated in the inner part of the aggregates, were processed as described by Crowther and Amos (14). In this way the digitized image is analyzed in terms of circular symmetric waves in order to find the relative composition of these harmonic components. This analysis makes use of the Fourier transform of the intensity data from the photographic plate. For the analysis of the end-on views special care was taken only to allow features of one projection to be transformed. Therefore the display of the digitized image was compared to the original micrograph and a circular mask was drawn around the projection which was analyzed. The density modulations within the mask were subjected to further analysis.

A typical result of a power spectrum of the rotational frequencies of a well-preserved particle is presented in Fig. 2b. It can be observed that there are clean maxima at 6 and 12 in the projected structure. The maximum modulations of the density occurred at radii from about 60-90 Å. At smaller radii no clear frequency maximum was found. The spectra of particles situated more at the outside of the aggregate, which generally exhibited a more rounded profile, did not show a clear maximum. Probably the preservation of a particle is better the more it is situated in the inside of the aggregate (11). The observed symmetry may as well depend on the length of the embedded particle. The helical form found to be present in the VRU preparations (see next section) has a much larger repeat than the stacked form. In the stacked form the symmetry of the projection adds up in register every 80 Å, whereas to observe the full end-on symmetry of the helical lattice a projection down 440 Å has to be realized. The detection of this symmetry is likely to depend on other factors, such as resolution of the staining technique, as a 34-fold modulation along a ring with a radius of roughly 75 Å may hardly be possible.

Optical Diffraction

General observations. Generally the optical transforms obtained from the virus particles exhibited a variable appearance, apart from the features discussed in the next sections. After examining a large number of micrographs for good particles in terms of straightness and equal width, and by diffracting these images, two kinds of particles were found. These will be called the stacked and the helical form. This nomenclature will be justified elsewhere. The two forms are found to be present in the preparations of the VRU strain. However, it is not known which of the two forms is dominant. Micrographs of particles from the 425 strain show characteristics similar to those of the stacked VRU

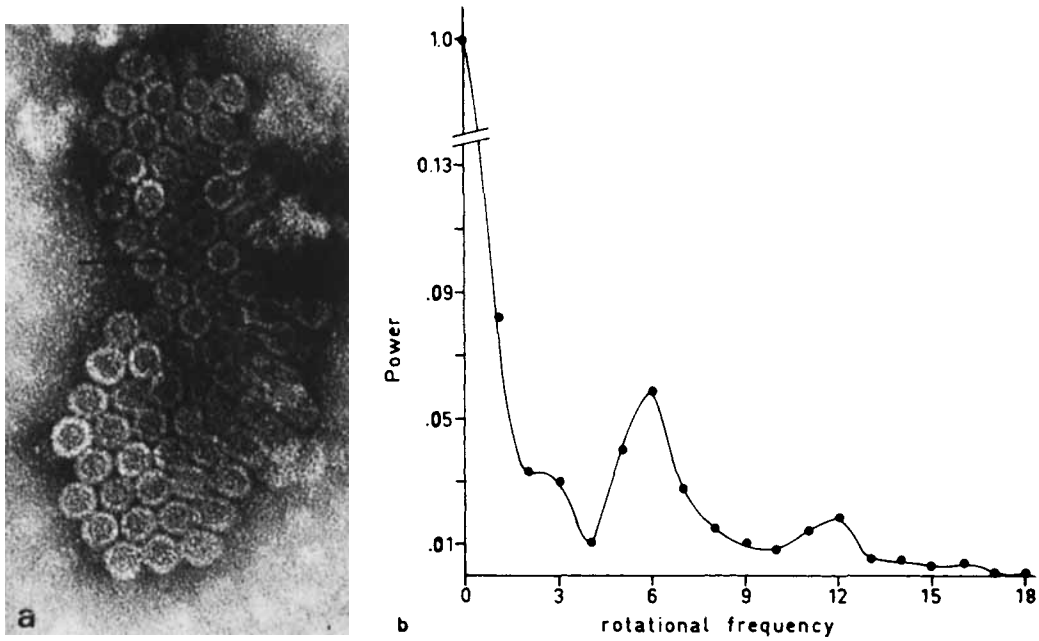

Fig. 2. a. End-on views on AMV particles of the strain 425. Negative stain is 1% uranylacetate solution. The aggregates were prepared by the addition of $MgCl_2$ to the virus suspension. Magnification: 22.10^4 X. b. A power spectrum of the Fourier amplitude derived from the particle indicated by the arrow. Clear maxima are present at frequencies of 6 and 12.

type. Also Gibbs et al. (2) and Hull et al. (3) have observed particles of the stacked type. Whether the polymorphism also exists in the 425 strain cannot be answered yet. Due to the very low signal-to-noise ratio of the optical transforms of these relatively short particles obtained so far, no reliable conclusions can be drawn.

The presence of at least two forms has been discovered by optical diffraction. Whether the polymorphism has been created by the preparation technique cannot be answered here. Additional support can be obtained by using other preparation methods as, for example, freeze etching and critical point drying. However, the observation that fixed virus particles contrasted with different stains exhibit the polymorphism strongly points to an existing structural difference rather than one induced by the preparation technique.

The stacked form. In fields of VRU particles generally one is able to recognize particles which exhibit a banded stain distribution and particles with a typical "zig-zag" stain modulation along their length. In Fig. 3a and 3c two examples are shown. This morphology, especially the "zig-zag" modulation, never comprises the total length of the particle, but varies from stretches of about 240 Å to 720 Å. No doubt, this phenomenon expresses the structural stability of the virus under the conditions of preparation, which is also apparent from the variability of many transforms investigated. The particles with the "zig-zag" pattern and those of the banded type occur on carbon foils as well as in stain over holes. The explanation for this appearance must be that there is a different orienta-

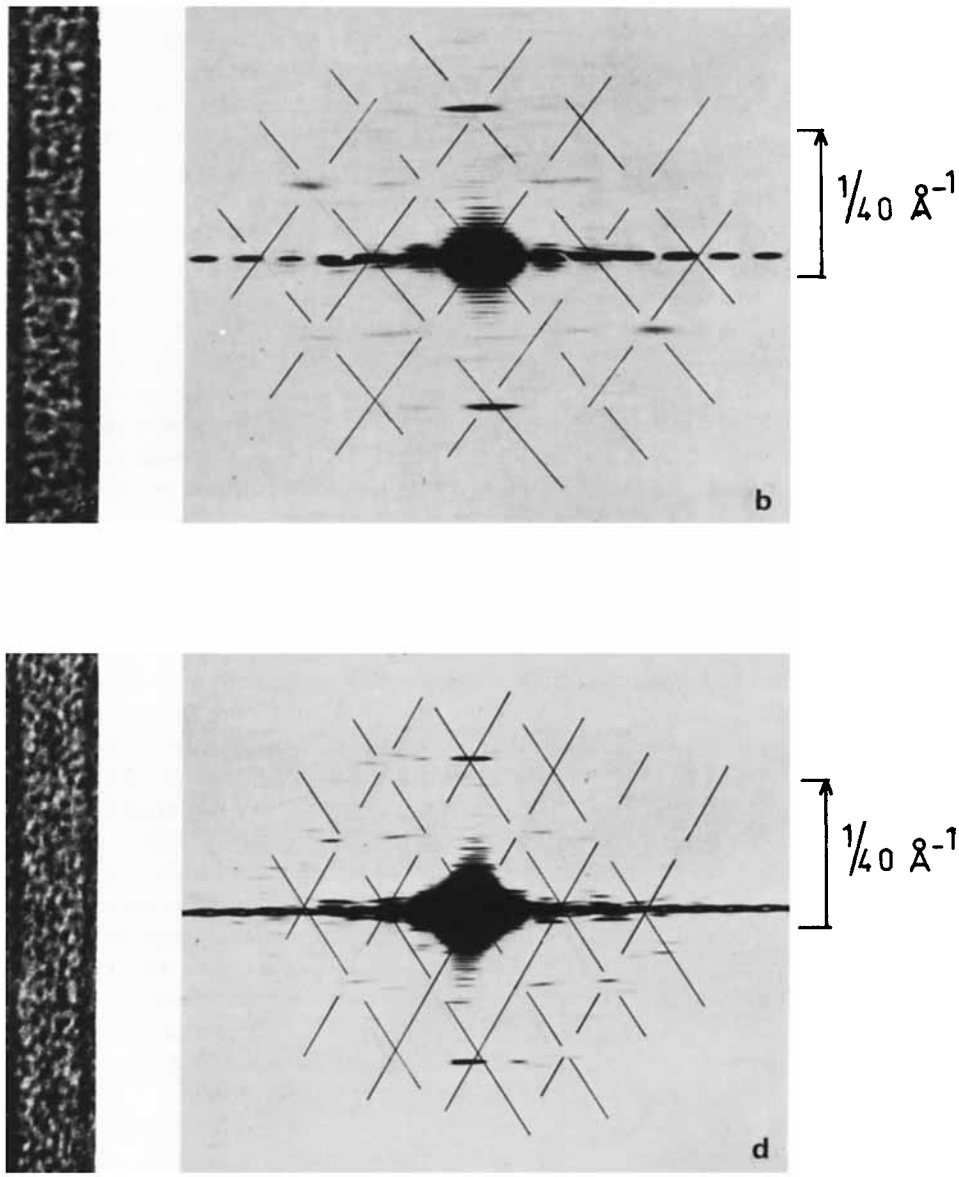

Fig. 3. Examples of AMV particles (VRU) of the stacked type (a) and (c) and their corresponding transforms (b) and (d). In the particle shown in (a) the morphological units are clearly visible. The strong meridional spacing in both transforms is present at a spacing of 1/40 $Å^{-1}$. In both transforms approximate hexagonal nets have been drawn. Particles over holes in stain. Magnification: 6.6×10^5.

tion of the particles with respect to the electron beam.

The "zig-zag" patterns can be described as consisting of rings of protein filled with stain. The centers of these rings, when connected, roughly define a set of equilateral triangles with sides measuring about 80 Å. It is known that dominant image features in negatively stained particles arise through the in-register superposition of near and far sides (15). As the "rings" occur on particles over holes, a condition which gives rise to double-sided images, the cylindrical symmetry of the particle must be odd.

In the diffraction patterns the intensity maxima fall on a set of layerlines, which can be indexed as orders of 80 Å. There is always a very strong 40 Å meridional maximum on the second layerline, which corresponds to the axial spacing of successive annuli of the particle (see Figs. 3b and 3d). Two of these annuli comprise a repeating unit, which, when stacked on top of each other, form this type of structure. On the basis of this repeat one would expect the particle to have a diameter of 132 Å. This number is clearly a minimum value as it has been derived from a lattice constant of a projected structure. It is reasonable to assume that the protein may extend radially from this lattice, giving rise to a larger value of the diameter. In fact the value of 150 Å found for particles over holes is likely to be a more realistic value for the diameter than the 132 Å derived from a 80 Å repeat. On the other hand if the particle had been flattened completely a diameter of about 207 Å would have been measured. This indicates that the situation on carbon is between that of a totally flattened and a perfect circular virus rod embedded in stain.

Figs. 3b and 3d shows approximate hexagonal nets drawn in the transforms. These lattices appear to fit the maxima reasonably well. In order to deduce the n-l plot of the diffraction pattern, the symmetry of the structure has to be known (16). A comparison of the molecular weight of a hypothetical structure built from one kind of protein with a molecular weight of 25,000 daltons places in a cylindrical hexagonal lattice with uneven symmetry and the experimental number for this strongly points to a 3-fold symmetry (see Fig. 8). The existence of a 3-fold, rather than a 5- or 7-fold symmetrical arrangement, finds additional support from the radial distances of the maxima in the optical transforms and the end-on views. The 6-fold nature of the latter can be considered to be pseudo-symmetry of a projected structure with a 3-fold symmetry. The radial distances of the maxima on the first layerline in a number of transforms favorably compare with a series of J_3 and J_9 rather than J_5 and J_{15}. For example the midpoint of the second maximum on $l = 1$ in Fig. 3b corresponds to the argument $2\pi Rr = 13$ for the maximum particle radius. This is a transform derived from a particle in stain over a hole, with $r = 75$ Å, therefore this value must be due to a J_9 rather than a J_{15}.

The n-l plot derived in this way is presented in Fig 5, together with the surface lattice in which the most prominent helical families are indicated. The selection rule is given by $l = n' + 2m$, in which $n' = 3n$. There are 6 unit cells in a repeat distance of 80 Å.

In terms of the helical diffraction theory (16) the n-l plot predicts interference of Bessel terms in the transforms. The intensity at each lattice point has a contribution derived from two cylindrical waves, each originating from a different side of the particle and each with a phase depending on the particle orientation. This explains the variations seen in many of the transforms and the examples given by Hull et al. (3). For example in a view down a 6-fold axis the G_3 and $G_{\bar{3}}$ terms on $l = 1$ will cancel as they are in antiphase, whereas in a view of the structure down a 2-fold axis these terms will add up with equal phases.

The helical form. The distinctive feature of the optical transforms of this type of structure is the existence of a pair of strong off-meridional maxima at a layerline of about 1/40 $Å^{-1}$ (see Fig. 4b and 4d), compared with the meridional maximum at the same reciprocal distance in the stacked structure.

For the indexing of the diffraction patterns use was made of numerical Fourier transforms, calculated from the intensity data. The phase differences of meridional-symmetric maxima of the calculated Fourier components can be used to draw conclusions concerning the odd-or eveness of the cylindrical waves in the projection and therefore support the assignment of Bessel orders (13). The phase differences of the maxima in a number of computed transforms on the layerlines at 1/40 and 1/44 $Å^{-1}$, within 30 degrees, correspond to even Bessel functions. An example of the magnitude of the Fourier components on these layerlines is presented in Fig. 6. Of all the transforms analyzed, these two maxima are the most consistent features and therefore are the best starting point for the indexing.

The radial distances of the maxima on the layerlines at about 1/40, 1/44, and 1/47 $Å^{-1}$, all lying on a lattice line (see Fig. 4), were, respectively, 1/145, 1/53, 1/32 $Å^{-1}$ as an average from 20 transforms. The result of the analysis is presented in Table I. From the phases of the maxima on the layerlines at 1/40 and 1/44 $Å^{-1}$ the presence of even Bessel functions can be deduced and therefore the maxima on this lattice line should be even. For this reason only ($2\pi Rr$) values for the maxima of a number of even Bessel orders have been tabulated. The basis for the comparison of the experimental maxima and the theoretical ones lies in the experimental radius of 75 Å over holes. Even with a small increase in this radius the experimental Bessel arguments indicate the presence of a J_2, J_8, and J_{14} on the respective layerlines rather than a series of J_2, J_6, and J_{10} or J_2, J_{10}, and J_{18}.

The indexing can be performed if the layerline separation is known. Although this number can be estimated from the layerline positions on which the J_2, J_8, and J_{14} are situated, the transforms were analyzed for the presence of a meridional maximum to find additional support. As the resolution at which this contribution is expected approximates the limits of the staining technique, only in a small number of transforms has this feature been found. A clear example is given in Fig. 4f, although in many transforms this contribution, to a weaker extent, is pertinently present.

The experimental meridional maxima were present at a spacing of about 1/26 $Å^{-1}$. On the basis that this maximum is a 17th order of a repeat of 440 Å the pattern can be indexed. In Fig. 4 two examples are given of the helical nets from one side of the particle, drawn in the transforms. Alternative indexing schemes have been tried but all of them were less plausible than the one proposed, as only this scheme accounts for the strongest and constant features of the diffraction patterns. The selection rule derived is given by $l = 6n' - 17m$, with $n' = 2n$, implying a 2-fold cylindrical symmetry. The n-l plot and the surface lattice with some of the prominent helical lattice lines are presented in Fig. 7.

DISCUSSION

The evidence obtained from the surface lattice of the protein coat of AMV strongly points to the existence of a cylindrical P_6 lattice. Together with the chemical data concerning the coat protein, this allows one to derive some structural implications. It is known that there is only one kind of polypeptide chain engaged in the formation of the coat.

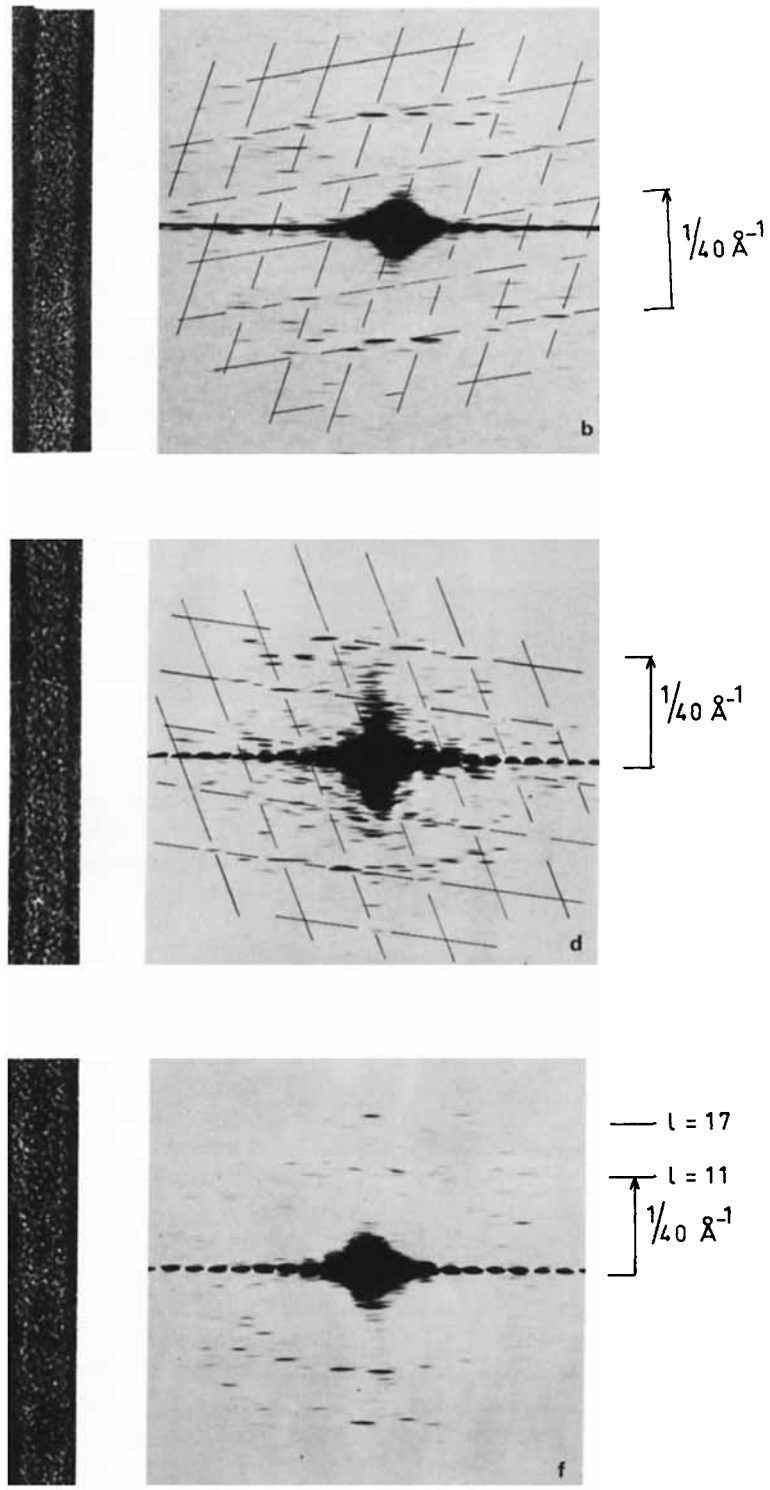

Fig. 4. Examples of AMV particles (VRU) of the helical type (a, c, and e) and their corresponding transforms (b, d, and f). In all the transforms a clear off-meriodional intensity contribution is present at a spacing of 1/40 $Å^{-1}$. In (b) and (d) approximate hexagonal nets, corresponding to one side of the particle, have been drawn. In the transform shown in (f) a clear meridional maximum is present at about 1/26 $Å^{-1}$. Particles on carbon. Magnification in (a) and (c): 5.0×10^5. Magnification of (e): 5.5×10^5.

TABLE I. A Comparison Between Theoretical and Experimental Maxima for Bessel Arguments, J_n (2π Rr), for the Helical Variant

Layerline Distance	Radial Distance of Maximum (Average of 20 Transforms)	2π Rr for r = 75 Å	Theoretical Values for 2π Rr in Case of a Perfect and Flattened Helix, Respectively (Ref. 17)
1/40 $Å^{-1}$ (l = 11)	1/145 $Å^{-1}$	3.3	J_2 : 3.1 – 2.3 J_4 : 5.3 – 4.1
1/44 (l = 10)	1/53	8.9	J_6 : 7.5 – 6.1 J_8 : 9.6 – 8.1
1/47 (l = 9)	1/32	14.7	J_{10} : 12.1 – 10.0 J_{12} : 13.9 – 12.0 J_{14} : 16.0 – 14.0

The molecular weight of this protein is 25,000 daltons as determined under conditions which favor dissociation of the protein (6). Under mild conditions, the virus can be dissociated into RNA and a protein component which appears to be a dimer of the 25,000 dalton unit. The dimers together with the RNA are capable of forming the nucleoprotein particle (18). Therefore it is highly likely that the dimer functions as the asymmetric unit in the surface lattice. From length measurements by electron microscopy and physical chemical data it is possible to calculate the molecular weight of the protein capsid per unit length (see Fig. 8). If the dimer axis coincides with the dyad positions of the lattice, then the molecular weight of the structure agrees well with the experimental value. In Fig. 9 the dimer has been drawn schematically in this position. It must be stressed that both the orientation and the shape of the dimer are not known yet.

The distribution of protein is such (Fig. 9) that the centers of the morphological units coincide with the hexamer positions of the lattice. In the model of Gibbs et al. (2), the protein is situated at the trigonal positions, whereas Hull et al. (3) derived a lattice with hexamer, clustering of a protein with a molecular weight of about 60,000. Moreover the lattice postulated by the first group of workers has to be rotated 90 degrees in order to fit the lattice derived here.

The different length of the AMV particles is likely to result from their RNA content. It is known that in AMV-425 the components contain a RNA molecule of a specific molecular weight (19). The P_6 lattice can be made of the required length by conversion of the 6-fold lattice points into 5-fold ones so that icosahedral caps are formed (4). The smallest component in the series will be an icosahedron made from 30 dimers.

It can be observed that the cells in the helical and the stacked form are roughly isomorphous, although their similarity has still to be quantified. However, at this stage it is tempting to speculate about the possible relationship between the two lattices. If the stacked lattice dislocates over one repeat in the axial direction, a helical type of lattice results. Similar structural arrangements have been observed in the case of other virus structures (see for example Refs. 20 and 21).

In this way the family (0, 2) in the stacked lattice is converted to a helical family, which might be represented by the $(\bar{2}, 11)$ family in the helical form. These reflections are the strongest features in the optical diffraction patterns of both types of structures. In a similar way the family (3, 1) transforms into the (4, 5) family of the helical lattice.

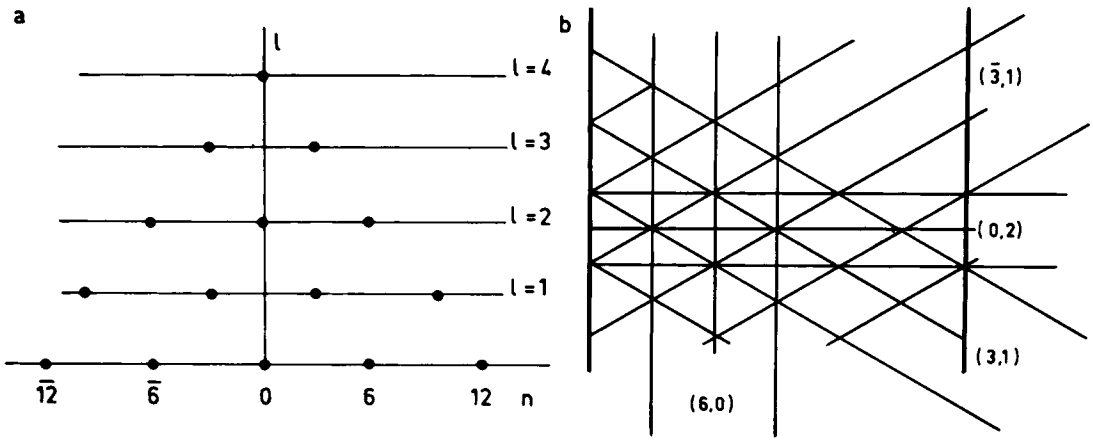

Fig. 5. The n-l plot and surface lattice for the stacked type of lattice. a. The n-l plot is given by the selection rule $l = n' + 2m$ with $n' = 3n$. Layerlines are equally spaced at intervals of $1/80$ Å^{-1}.
b. The surface lattice with the most dominant helical families. The spacing of (0, 2) corresponds to 40 Å, the distance between successive rings in the structure.

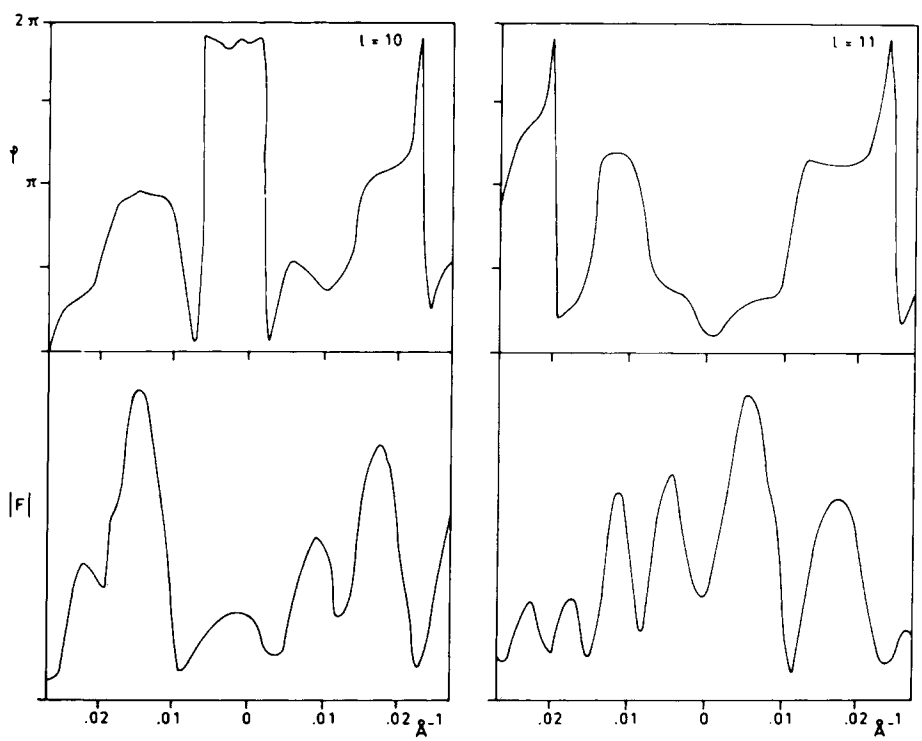

Fig. 6. The amplitudes and phases in the computed transform derived from the particle shown in Fig. 3c. The phases of the maxima on the layerlines $l = 10$ and $l = 11$ suggest the presence of even Bessel functions.

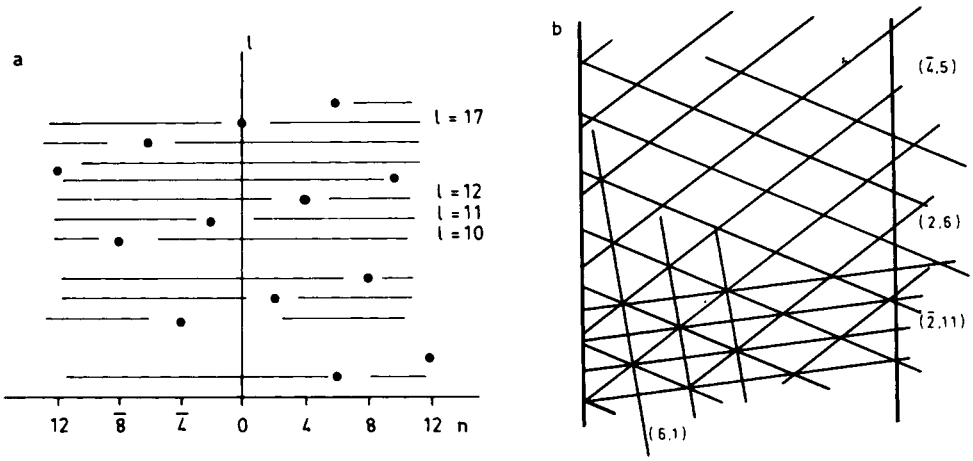

Fig. 7. The n-l plot and the surface lattice for the helical type of lattice. a. The n-l plot is given by the selection rule $l = 6n' - 17m$ with $n' = 2n$. Layerlines are equally spaced corresponding to a repeat of 440 Å. b. The surface lattice with the most dominant helical families. The hand of the helices is arbitrary. The spacing of the family ($\bar{2}$, 11) corresponds to 40 Å and has to be compared with the (0, 2) helices in the stacked type of lattice.

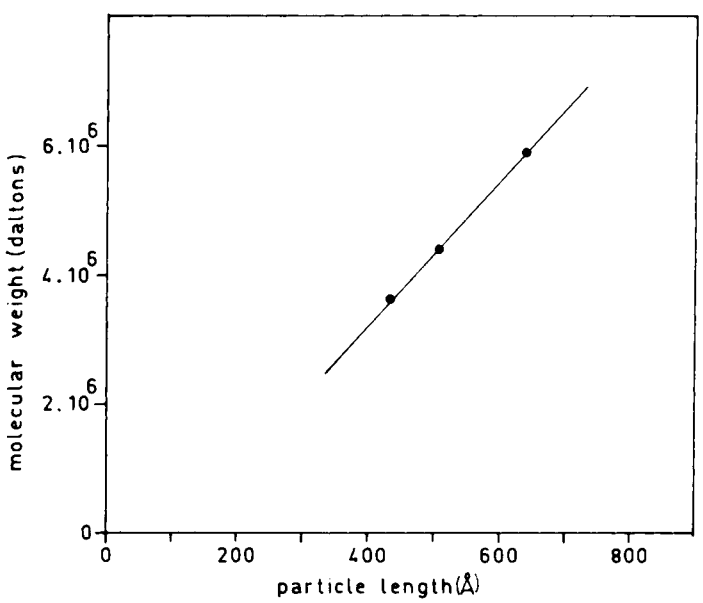

Fig. 8. A plot of the molecular weight of AMV–425 protein components versus their length. The length of the particles was obtained from Ref. 10. The molecular weights were determined by sedimentation equilibrium measurements. These data were kindly provided by Dr. R. A. Heytink (to be published). For the calculation of the molecular weights of the RNA free capsids it was assumed that the particles consist of 83% protein. From the slope of the line through the three points a molecular weight of 9×10^5 daltons of a cylindrical shell of 80 Å length can be derived. For a hexagonal lattice with 3–, 5–, and 7–fold symmetry the theoretical molecular weight amounts to 9×10^5, 1.5×10^6, and 2.1×10^6, respectively, on the basis of a unit of 25,000 daltons. Therefore, this calculation unequivocally shows that the symmetry is 3–fold. The outcome of the molecular weights is not affected by the assumption that polymorphism exists, as both lattice types have the same number of unit cells per unit length within experimental error.

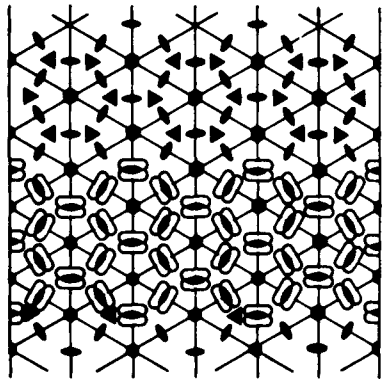

Fig. 9. A schematic drawing of the dimers in the surface lattice. The protein is situated such that the lattice dyad coincides with the 2–fold axis of the protein dimer. The orientation of the dimer in the lattice, as well as its 3– dimensional shape, are not known.

Whether this kind of transition is the basis for the polymorphism of the protein coat has to be supported by transforms with a higher signal-to-noise ratio derived from images of better preserved paticles. The selection rule determined for the helical lattice does not support the existence of a hexagonal lattice dislocated in the way described, as can be determined from studies with geodestic models.

At this moment the reason for the existence of the polymorphism is not understood. Even the question whether it is the conformation of the RNA which changes the bonding properties of the protein or whether it is the protein alone causing the structural differences cannot be answered. Because of this, the postulated slippage of the lattice might as well be highly disputable. The structural basis for the capping of the tubes is in the same way an open question, as no experimental evidence is available yet to deduce the clustering pattern of the protein. An approach to this last problem could be a study of the *in vitro* assembled products, as preliminary experiments have indicated, that under certain conditions the virus protein forms regular spherical particles with a diameter similar to the tubular forms. In view of this we have not considered it fruitful to examine this question exhaustively.

In order to obtain more information about the distribution of protein within the unit cell, filtering experiments are in progress. The stacked form has an unfavorable lattice for this kind of study, as in general both sides of the structure cannot be synthesized separately. In the same way the helical form is the most suitable structure for a 3–D reconstruction, as in this case, contrary to the stacked form, no overlapping Bessel functions occur (23).

ACKNOWLEDGMENTS

The authors have been allowed to use a number of computer programs from the MRC Laboratory of Molecular Biology in Cambridge for which they are very thankful.

The expert assistence of Truus Remmelzwaal with the programming and scanning facilities provided by Dr. van der Ploeg are gratefully acknowledged.

REFERENCES

1. Kelley, J. J., and Kaesberg, P. Biochim. Biophys. Acta 55:236 (1962).
2. Gibbs, A. J., Nixon, H. L., and Woods, R. D. Virology 19:441 (1963).
3. Hull, R., Hills, G. J., and Markham, R. Virology 37:416 (1969).
4. Caspar, D. L. D. and Klug, A. Cold Spring Harbor Symp. Quant. Biol. 27:1 (1962).
5. Hull, R. Virology 42:283 (1970).
6. Kruseman, J., Kraal, B., Jaspars, E. M. J., Bol. J. F., Brederode, F. Th., and Veldstra, H. Biochemistry 10:447 (1971).
7. Bol, J. F. and Veldstra, H. Virology 37:74 (1969).
8. van Domelen, B. H. and Beeman, W. W. Biochim. Biophys. Acta 61:872 (1962).
9. van Vloten-Doting, L. and Jaspars, E. M. J. Virology 48:699 (1972).
10. van Vloten-Doting, L., Dingjan-Versteegh, A. M., and Jaspars E. M. J. Virology 40:419 (1970).
11. Hull, R., Hills, G. J., and Plaskitt, A. J. Ultr. Res. 26:465 (1969).
12. Kay, D., Techniques for Electron Microscopy, Oxford, Scientific Publications (1972).
13. DeRosier, D. J. and Moore, P. B. J. Mol. Biol. 52:355 (1970).
14. Crowther, R. A. and Amos, L. A. J. Mol. Biol. 60:123 (1971).
15. Finch, J. T. and Klug, A. J. Mol. Biol. 15:344 (1966).
16. Klug, A., Crick, F. H. C. and Wyckoff, H. W. Acta Cryst. 11:199 (1958).
17. Moody, M. F. J. Mol. Biol. 25:167 (1967).
18. Bol, J. F. and Kruseman, J. Virology 37:485 (1969).
19. Bol, J. F., van Vloten-Doting, L. and Jaspars, E. M. J. Virology 46:73 (1971).
20. Kiselev, N. A. and Klug, A. J. Mol. Biol. 40:155 (1969).
21. Leonard, K. R., Kleinschmidt, A. K., Agabian-Keshishian, N., Shapiro, L. and Maisel, J. V. J. Mol. Biol. 71:201 (1972).
22. Goodman, J. W. Introduction to Fourier Optics, London, McGraw-Hill (1968).